Original Article

Institution of MECHANICAL ENGINEERS
Journal of POWER AND ENERGY

Proc IMechE Part A:
J Power and Energy
2016, Vol. 230(2) 219–233

DOI: 10.1177/0957650915619561
pia.sagepub.com
SAGE

Optimal management of a solar power plant equipped with a thermal energy storage system by using dynamic programming method

Javad Mahmoudimehr and Leila Loghmani

Abstract

This study employs the dynamic programming (DP) optimization approach to maximize the daily revenue of a concentrating solar power plant (CSP) equipped with a thermal energy storage system (TES). DP guarantees the optimal solution and is easy from the computer coding point of view; therefore, it can be of great importance. Two real-life case studies are considered. The first case has a simple thermal model and is mainly chosen in order to verify the present optimization program. In this case, the present work achieves 1.3% (or US$480 /day) higher daily revenue in comparison with the literature. However, the simple thermal model of the first case study cannot appropriately simulate the actual operation of a CSP. Therefore, the optimization was applied to another case with a more detailed thermal model. The findings indicate that in order to maximize revenue, the charging and discharging of the TES should be managed such that the power block works under base load conditions (whenever it is active) and during periods of high electricity prices, regardless of the level of the daily solar radiation pattern. Furthermore, quantitative investigations show the substantial influence of the TES system on the daily revenue, especially for the case of low solar radiation pattern.

Keywords

Solar power plant, energy storage system, performance optimization, dynamic programming method

Date received: 30 July 2015; accepted: 2 November 2015

Introduction

The growing global energy demand, the depletion of fossil fuel resources in the coming decades, and environmental issues related to the consumption of fossil fuels necessitate paying special attention to the renewable energy sources.

Solar energy received by the Earth during an hour equals the yearly global energy demand. However, only about 1% of the global energy demand is directly supplied by the solar radiation.[1]

Concentrating solar power plants (CSPs) possess some advantages over other renewable systems. They can include a TES and can be coupled with conventional power-generating technologies.[2] Moreover, deserts or arid regions are the best sites for installing CSPs; therefore, these systems are not subject to land use issues or controversies.[3] At present, there are 29 active CSPs in the world with a total power of 1220 MW-e, and also 31 CSPs are being installed.[4,5] Estimations show that the installed capacity of CSPs will reach ~37 GW by 2025, preventing the emission of 362 million tons of CO_2 per year.[6,7]

On the other hand, the high investment costs of CSPs, and the variability of solar radiation constitute the main drawbacks of employing such solar systems. Including TES systems into CSPs can help moderate these problems through managing production times.[2,8,9] Design and performance optimizations of CSPs are other ways of making the solar systems more viable and have been the subject of several recent research works.

To minimize the levelized cost of energy (LCOE), Montes et al.[10] examined five solar plants with the same power blocks (PBs) but different solar field (SF) sizes, and it was concluded that a plant without a TES system should not have a large SF size. Dominguez et al.[2] used the mixed-integer linear programming (MILP) method to maximize the revenue of a CSP with a TES system. Uncertainty in SF thermal power production and the volatility of market

Department of Mechanical Engineering, Faculty of Engineering, University of Guilan, Rasht, Iran

Corresponding author:
Javad Mahmoudimehr, Department of Mechanical Engineering, Faculty of Engineering, University of Guilan, P.O. Box 3756, Rasht 41996-1376, Iran.
Email: mahmoudimehr@guilan.ac.ir

prices were considered in this work. Lizarraga et al.[11] employed the nonlinear programming (NLP) approach to optimize the operation of a CSP with a TES system. The results indicated that production scheduling is more profitable under highly fluctuating electricity price scenarios. Martín and Martín[12] used the NLP method to optimize year-round operation of a CSP in Almeria of Spain. The obtained LCOE was higher than that of fossil-fuel based plants. However, the scale-up investigation revealed that the production cost can be reduced if solar capacity approaches that of conventional power facilities. Kost et al.[13] used the mixed integer optimization approach to find the optimal sizes of the SF and storage system of a Spanish CSP. The results indicated that the current Spanish support scheme offers only limited incentives for large thermal storage capacities. Baghernejad and Yaghoubi[14] employed the genetic algorithm (GA) for the exergo-economic optimization of an integrated solar combined cycle system. This attempt led to reductions in the LCOE and the exergy destruction cost. SF size, TES capacity, and the power of auxiliary system constitute the design parameters of a research work conducted by Cabello et al.[15] to maximize the yearly profit of a solar plant by using GA. For a gross power of 50 MW, the values of 19.3 M€/year and 18.5 c€/kWh were obtained for the economic profit and LCOE, respectively. Soltani et al.[16] address the multiobjective optimization of a solar-hybrid cogeneration cycle by using GA. This attempt resulted in considerable reductions in fuel consumption and chemical exergy destruction. Thermo-economic optimization of a solar plant by using mimetic algorithms was presented by Silva et al.[17] In this work, the optimization based on life cycle savings suggested larger plants but lower SF efficiencies; however, these observations were reversed for the optimization based on payback time. Marano et al.[18] applied the dynamic programming (DP) method to optimize the performance of a hybrid power plant consisting of a wind farm, a photovoltaic system, and a compressed air energy storage system (CAES). It was observed that the CAES technology can help to achieve a higher power density in the wind farm through generating a high-speed artificial wind; moreover, it can help to decrease the uncertainty in the electricity generation resulting from unpredictable weather conditions.

The general form of an optimization problem is shown in equation (1), where f is the objective function, h_j and g_k represent the equality and inequality constraints, and $x = (x_1, x_2, \ldots, x_n)$ denotes the decision vector. Also, subscripts L and U stand for the lower and upper bounds of each decision variable.

Maximize (or minimize) $f(x)$ Subject to

$$\begin{aligned} &h_j(x) = 0, \quad (j = 1, 2, \ldots, J) \\ &g_k(x) \leqslant 0, \quad (k = 1, 2, \ldots, K) \\ &x_{i,L} \leqslant x_i \leqslant x_{i,U}, \quad (i = 1, 2, \ldots, n) \end{aligned} \tag{1}$$

In general, the objective and constraint functions can be nonlinear or linear, and the decision variables can be continuous, discrete or mixed (commonly called mixed integer). In many nonlinear optimization problems, the objective function has a large number of local optima. This is also the case for the mixed integer linear or nonlinear problems.[19] A local optimum is a selection from a given domain which is only better than the neighboring selections. By contrast, a global optimum is better than any other selection in a given domain. Finding the global optimum is much more difficult than finding a local optimum.

There are many optimization algorithms in the literature; however, no single algorithm is suitable for all problems, as dictated by the No Free Lunch Theorems,[20] and the selection of an appropriate algorithm highly depends on the problem under consideration. A brief introduction to the primary types of optimization approaches together with their positive and negative points is provided below.

Gradient-based algorithms use the information of derivatives to approach the optimal solution. These algorithms are very efficient local search methods; however, they can be typically trapped in a local optimum, and they are complex algorithms to implement.[20–22] Furthermore, in most problems, the gradient information is not readily available (i.e. when the objective function is discontinuous or cannot be expressed explicitly) and needs to be approximated by using finite difference methods.[21,22]

Evolutionary algorithms (such as GA, particle swarm optimization, and Tabu search) are inspired by some phenomena from nature. These methods do not require any gradient information and are easy to implement.[21,23,24] Moreover, they have a much better chance of finding the global or near global optimum than the local algorithms described earlier. The big drawbacks associated with these algorithms are high computational cost, poor constraint-handling abilities, problem-specific parameter tuning and limited problem size.[21] These algorithms work in a stochastic manner; i.e. they usually reach a different solution every time they are executed.[20]

The DP method is a gradient-free optimization technique invented by an American mathematician named Bellman.[25] This method makes use of a simple and elegant idea and solves a complex problem by breaking it down into a collection of simpler subproblems. The DP method is not sensitive to the nonlinearity and discontinuity of the problem, cannot be trapped in a local optimum, and is guaranteed to find the global optimum. Moreover, this method is easy from the computer coding point of view. The main drawback of this method is that it is only applicable to the problems exhibiting the properties of overlapping sub-problems.[18,25–27]

In general, the problem of optimizing the performance of a CSP with a TES system over a period of time is nonlinear because it has nonlinear governing

equations and is mixed integer since it includes integer variables (on/off state of the CSP in each time interval) in addition to continuous variables. None of the local and evolutionary algorithms can guarantee the global optimum for such a complex mixed integer nonlinear problem. In some research works (such as that of Dominguez et al.[2]) the complexity of the problem was reduced through considering a simple linear thermal model of the CSP.

However, as mentioned previously, the DP method guarantees the global optimal solution if it is applicable to a problem. This study employs the DP method to optimize the daily operation of a CSP equipped with a TES system. To verify the present approach, it is applied to a benchmark case study with a linear thermal model presented by Dominguez et al.,[2] and the results are compared to those of Dominguez et al.[2] obtained from the MILP approach (which lies in the category of the local search algorithms). However, this simple thermal model does not suffice to accurately simulate the real operation of a CSP; therefore, in the next step, another case with a more detailed thermal model is considered. For this case, the influence of the TES system on the CSP performance as well as on the daily revenue is quantitatively investigated for different solar radiation patterns (from low to high levels).

The main contributions of this paper to the subject are as follows:

Employing the DP method to optimize the quasi-steady operation of a CSP with a detailed thermal model. The present approach guarantees the optimal solution and is easy from the computer coding point of view; moreover, it is not limited to CSPs with TES systems, but rather it can be applied to the various types of solar plants with various types of storage systems and different objective functions.

Quantitatively investigating the influence of a TES system on the optimal performance strategy and daily revenue of a CSP under different levels of solar radiation patterns (from low to high level).

The rest of this paper is organized as follows. The case studies with their governing equations are described in the next section. The third section describes the DP approach. Results are discussed in the penultimate section, and the paper ends with conclusions.

Case studies

First case study (benchmark)

A simple thermal model of IBERDROLA[2] (a grid connected CSP located in Puertollano, Spain) is considered for the first case study. Figure 1 schematically shows the primary elements of the CSP as black boxes (i.e. without their internal components). Regarding Figure 1, the SF converts solar radiation to the thermal power ($\dot{Q}^S$). Then, $\dot{Q}^S$ is either delivered to the PB ($\dot{Q}^{SP}$) to generate electricity or sent to the TES section ($\dot{Q}^{ST}$) to be stored. The thermal power required by the PB to generate electricity can be supplied by either the SF or the TES system ($\dot{Q}^{TP}$).

The objective function and constraints of the problem are listed in the following equations

$$Max\left(\sum_{t=1}^{24} f_t = Price_t \cdot P_t^{Total}\right) \tag{2}$$

$$P_t^{Total} = \eta_1 \cdot \dot{Q}_t^{SP} + \eta_2 \cdot \dot{Q}_t^{TP} \tag{3}$$

$$\dot{Q}_t^{SP} + \dot{Q}_t^{ST} = \dot{Q}_t^{S} \tag{4}$$

$$Q_t^{T} = Q_{t-1}^{T} + \eta_3 \cdot \dot{Q}_t^{ST} - \dot{Q}_t^{TP} \tag{5}$$

$$0 \leqslant P_t^{Total} \leqslant P^{max} \tag{6}$$

$$\dot{Q}^{P,min} \cdot U_t \leqslant \dot{Q}_t^{SP} + \dot{Q}_t^{TP} \leqslant \dot{Q}^{P,max} \cdot U_t \tag{7}$$

$$Q^{T,min} \leqslant Q_t^{T} \leqslant Q^{T,max} \tag{8}$$

$$\eta_3\left(\dot{Q}_{t+1}^{ST} - \dot{Q}_t^{ST}\right) \leqslant R^{Ch} \tag{9}$$

$$\eta_2\left(\dot{Q}_t^{TP} - \dot{Q}_{t+1}^{TP}\right) \leqslant R^{Dis} \tag{10}$$

$$\dot{Q}_t^{TP}, \dot{Q}_t^{SP} \geqslant 0 \tag{11}$$

$$|U_t - U_{t-1}| + \left|U_t - U_{t+1}\right| \leqslant 1 \tag{12}$$

Equation (2) defines maximum daily revenue as the objective, where $Price_t$ and P_t^{Total} denote electricity price and generated electrical power at period t, respectively. Herein, the quasi-steady assumption is used to simulate the unsteady operation of the CSP, and the whole day period is divided into 24 1-h intervals.

Equation (3) shows P^{Total} as a function of $\dot{Q}^{SP}$ and $\dot{Q}^{TP}$, where η_1 and η_2 denote the conversion efficiency of $\dot{Q}^{SP}$and $\dot{Q}^{TP}$ to electrical power, respectively.

Equation (4) shows the power balance among $\dot{Q}^{S}$, $\dot{Q}^{ST}$, and $\dot{Q}^{SP}$.

Equation (5) shows the energy balance in the TES section, where Q_t^T is the amount of thermal energy within the TES at the end of time interval t, and η_3 denotes the efficiency of converting $\dot{Q}^{ST}$ to Q^T.

Equation (6) defines the capacity of power generation.

Equation (7) specifies an allowable range for the total amount of thermal power received by the PB. In this equation, U takes 1/0 for the on/off state of the PB.

Equation (8) specifies an allowable range for the amount of energy within the TES section.

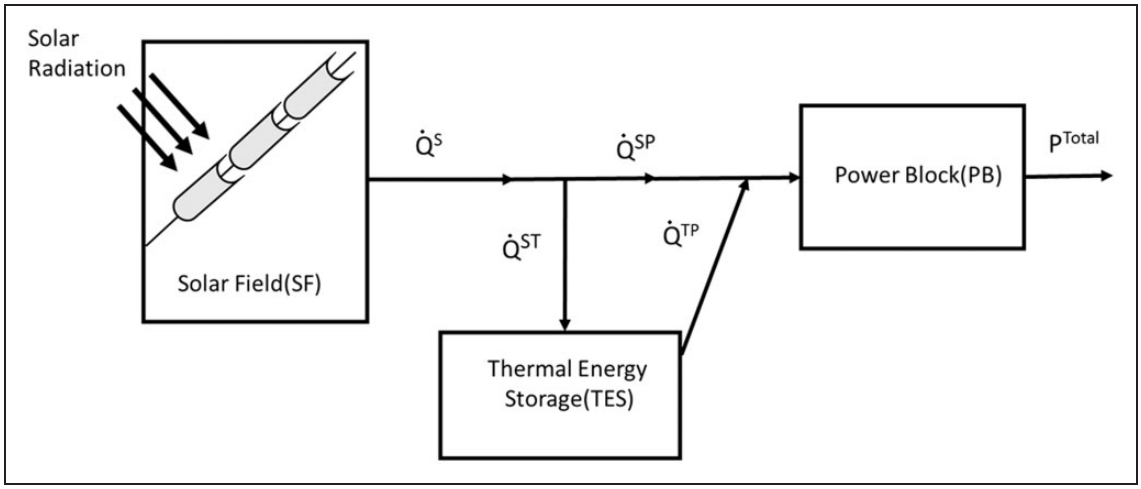

Figure 1. Schematic view of the first case study.

Table 1. Technical data for the first case study.[2]

P^{max} (MWe)	Q^{Pmax} (MW)	Q^{Pmin} (MW)	Q^{Tmax} (MWh)	Q^{Tmin} (MWh)	Q_0^T (MWh)	R^{Ch} (MWe/h)	R^{Dis} (MWe/h)	η_1	η_2	η_3
50	125	50	700	45	350	80	35	0.40	0.35	0.80

Equations (9) and (10) define the ramp-up and ramp-down limits for charging and discharging the TES, respectively.

Equation (11) indicates that $\dot{Q}^{TP}$ and $\dot{Q}^{SP}$ must be positive. Constraint (12) prevents the PB from frequently oscillating between the on and off states. To satisfy the inequality of equation (12), at least one of the two equalities of $U_t = U_{t-1}$ and $U_t = U_{t+1}$ must be valid. This implies that the on/off state of the PB must remain unchanged at least for two consecutive time intervals.

The amount of energy within the TES is considered to be the independent variable for each time interval; consequently, $[Q_1{}^T, Q_2{}^T, \ldots, Q_{24}{}^T]$ constitute the set of decision variables of the first case study.

The input data required for the first case study are gathered in Tables 1 and 2. The hourly data of SF thermal power production shown in Table 2 belongs to a representative summer day.

Table 2. SF thermal production and electricity price for the first case study.[2]

Time (h)	Q^S (MW)	Price ($/MWh)	Time (h)	Q^S (MW)	Price ($/MWh)
1	0	52.47	13	130	41.25
2	0	41.25	14	150	59.83
3	0	54.18	15	150	36.78
4	0	35.15	16	140	53.18
5	0	47.43	17	150	40.42
6	0	38.95	18	150	56.17
7	30	26.59	19	100	47.34
8	90	37.57	20	60	91.99
9	150	47.14	21	0	45.27
10	150	56.7	22	0	64.29
11	150	35.88	23	0	57.68
12	100	42.61	24	0	41.4

Second case study

Figure 2 schematically shows the elementary components of the Andasol-I[9] (a grid connected CSP located in Granada, Spain). This case was considered to be the second case study. It is perceived from Figures 1 and 2 that both of the first and the second case studies have the same primary elements including SF, TES, and PB. However, while these elements were assumed as black boxes in the first case study, they are considered with their major internal components in the second case study. There are still other secondary components omitted for the sake of simplicity.

Regarding Figure 2, ''Therminol VP1'' as the heat transfer fluid (HTF) is warmed up in the SF section. The hot HTF is then sent toward the TES for storing its thermal energy or toward the PB for generating electricity. During charge mode operation, at the heat exchanger of the TES, heat is transferred from the hot HTF to the solar salt travelling from the cold tank to the hot tank. This mechanism is reversed during the discharge mode operation. The PB section is a simple Rankine cycle receiving its required energy from the hot HTF passing through the boiler.

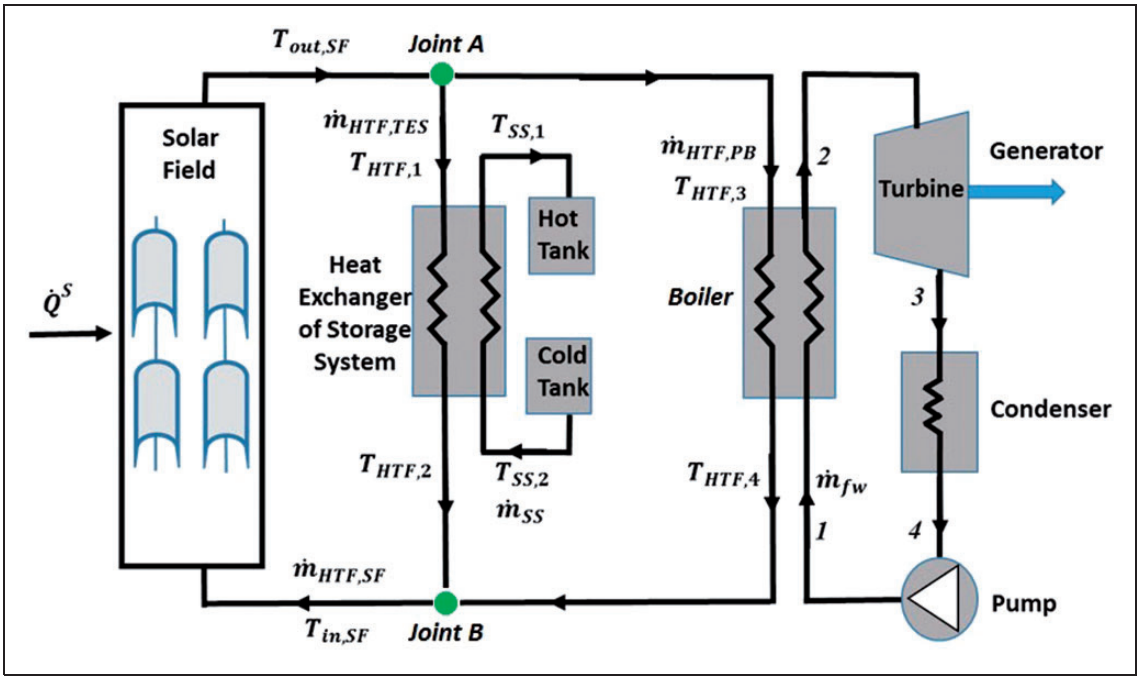

Figure 2. Schematic view of the second case study.

The objective function of the second case study is the same as that of the first one. Thermal modeling is carried out through solving a set of nonlinear equations by using the Newton–Raphson method. These equations are listed below and can be simply extended to the discharge mode operation.

Solar field section. For the present case study, SF thermal power production ($\dot{Q}^S$) can be estimated as a linear function of direct normal irradiance (DNI)[9]

$$\dot{Q}^S = 0.386\,DNI - 20.94 \tag{13}$$

The SF thermal power is transferred to the HTF, thereby increasing its enthalpy

$$\dot{Q}^S = \dot{m}_{HTF,SF}\left(h_{out,SF} - h_{in,SF}\right) \tag{14}$$

TES section. Equations (15) and (16) stand for the mass balance in the hot and cold tanks, respectively, where M_t^H and M_t^C denote the mass of the solar salt within the hot and cold tanks at the end of time interval t, respectively, and $\dot{m}_{ss}$ indicates the solar salt mass flow rate. Furthermore, subscripts t and $t+\Delta t$ represent two consecutive time intervals.

$$M_{t+\Delta t}^H = M_t^H + \dot{m}_{ss}\cdot\Delta t \tag{15}$$

$$M_{t+\Delta t}^C = M_t^C - \dot{m}_{ss}\cdot\Delta t \tag{16}$$

Equations (17) and (18) show the energy balance for the hot and cold tanks, respectively, where u denotes the specific internal energy of the solar salt within a tank, and $h_{ss,1}$ and $h_{ss,2}$ show the enthalpies of solar salts entering the hot tank and leaving the cold tank, respectively.

$$M_{t+\Delta t}^H\cdot u_{t+\Delta t}^H = M_t^H\cdot u_t^H + \dot{m}_{ss}\cdot\Delta t\cdot h_{ss,1} \tag{17}$$

$$M_{t+\Delta t}^C\cdot u_{t+\Delta t}^C = M_t^C\cdot u_t^C - \dot{m}_{ss}\cdot\Delta t\cdot h_{ss,2} \tag{18}$$

Equations (19) to (23) relate to the heat exchanger section of the TES. In these equations, $\dot{Q}_{exch,TES}$ is the heat transfer rate, $\dot{m}_{HTF,TES}$ denotes the mass flow rate of HTF passing through the heat exchanger, $h_{HTF,1}$ and $h_{HTF,2}$ are the enthalpies of HTF at the inlet and exit of the heat exchanger, respectively, $(U\cdot A)_{exch,TES}$ is the overall heat transfer coefficient multiplied by the heat exchanger surface area, and $\Delta T_{LM,TES}$ shows the logarithmic mean temperature difference. Moreover, subscript "des" denotes the value at design conditions. It is worth noting that equation (22) corrects the overall heat transfer coefficient for the off-design operating conditions.[9]

$$\dot{Q}_{exch,TES} = \dot{m}_{ss}\cdot\left(h_{ss,1} - h_{ss,2}\right) \tag{19}$$

$$\dot{Q}_{exch,TES} = \dot{m}_{HTF,TES}\cdot\left(h_{HTF,1} - h_{HTF,2}\right) \tag{20}$$

$$\dot{Q}_{exch,TES} = (U\cdot A)_{exch,TES}\cdot\Delta T_{LM,TES} \tag{21}$$

$$(U\cdot A)_{exch,TES} = (U\cdot A)_{exch,TES,des} \times \left(\dot{m}_{HTF,TES}/\dot{m}_{HTF,TES,des}\right)^{0.8} \tag{22}$$

$$\Delta T_{LM,TES} = \left[\left(T_{HTF,1} - T_{SS,1}\right) - \left(T_{HTF,2} - T_{SS,2}\right)\right] / Ln\left[\left(T_{HTF,1} - T_{SS,1}\right)/\left(T_{HTF,2} - T_{SS,2}\right)\right] \tag{23}$$

Power block section. Equations (24) to (28) relate to the boiler section where sub-cooled water is converted

to superheated vapor. In these equations, $\dot{m}_{fw}$ is the mass flow rate of working fluid (water), h_1 and h_2 indicate the inlet and outlet enthalpies of the water, respectively, $\dot{m}_{HTF,PB}$ shows the mass flow rate of HTF passing through the boiler, and $h_{HTF,3}$ and $h_{HTF,4}$ represent the inlet and outlet enthalpies of the HTF, respectively.

$$\dot{Q}_{exch,boiler} = \dot{m}_{fw} \cdot (h_2 - h_1) \tag{24}$$

$$\dot{Q}_{exch,boiler} = \dot{m}_{HTF,PB} \cdot \left(h_{HTF,3} - h_{HTF,4}\right) \tag{25}$$

$$\dot{Q}_{exch,boiler} = (U \cdot A)_{exch,boiler} \cdot \Delta T_{LM,boiler} \tag{26}$$

$$(U \cdot A)_{exch,boiler} = (U \cdot A)_{exch,boiler,des}\left(\dot{m}_{fw}/\dot{m}_{fw,des}\right)^{0.8} \tag{27}$$

$$\Delta T_{LM,boiler} = \left[\left(T_{HTF,3} - T_2\right) - \left(T_{HTF,4} - T_1\right)\right] / Ln\left[\left(T_{HTF,3} - T_2\right)/\left(T_{HTF,4} - T_1\right)\right] \tag{28}$$

The water pressure drop across the boiler is calculated by equation (29), where k_p is a constant coefficient.[10]

$$P_2 - P_1 = -k_p \cdot \left(\dot{m}_{fw}\right)^2 \tag{29}$$

Equations (30) to (33) govern the operation of the steam turbine. Equation (30) defines the turbine adiabatic efficiency (η_T) as a function of water enthalpy difference between the turbine suction and discharge sides. In this equation, subscript "s" represents the isentropic condition.

$$\eta_T = (h_2 - h_3)/\left(h_2 - h_{3,s}\right) \tag{30}$$

Equation (31) corrects the turbine efficiency for off-design conditions. In this equation, $\eta_{T,des}$ is the turbine efficiency at design conditions.[10]

$$\eta_T = \eta_{T,des} \cdot \left[1 - \begin{pmatrix} 0.191 - 0.409\left(\dot{m}_{fw}/\dot{m}_{fw,des}\right) \\ + 0.218\left(\dot{m}_{fw}/\dot{m}_{fw,des}\right)^2 \end{pmatrix}\right] \tag{31}$$

The power generated by the steam turbine is obtained as

$$\dot{W}_T = \dot{m}_{fw} \cdot (h_2 - h_3) \tag{32}$$

Equation (33) relates the turbine suction and discharge pressures, where the subscript "des" denotes a corresponding value at design conditions[10]

$$\left(P_2^2 - P_3^2\right)/\left(P_{2,des}^2 - P_{3,des}^2\right) = \left(\dot{m}_{fw}/\dot{m}_{fw,des}\right)^2 \tag{33}$$

It is assumed that no pressure drop occurs across the condenser and water leaves the condenser at the saturated liquid state.

Equations (34) to (36) govern the operation of the pump, where $\dot{W}_{pump}$ shows pumping power, $(P_1 - P_4)$ indicates the pressure rise across the pump, and υ_f is the liquid water specific volume. Equation (36) corrects the pump efficiency for off-design conditions, where $em_o$is a correction factor, and $\eta_{pump,des}$ denotes the efficiency at the design conditions.[10]

$$\dot{W}_{pump} = \dot{m}_{fw} \cdot \upsilon_f \cdot (P_1 - P_4)/\eta_{pump} \tag{34}$$

$$\dot{W}_{pump} = \dot{m}_{fw} \cdot (h_1 - h_4) \tag{35}$$

$$\eta_{pump} = \eta_{pump,des} \cdot \left[\begin{matrix} em_o + 2(1 - em_o)\left(\dot{m}_{fw}/\dot{m}_{fw,des}\right) \\ - (1 - em_o)\left(\dot{m}_{fw}/\dot{m}_{fw,des}\right)^2 \end{matrix}\right] \tag{36}$$

The net generated power is obtained as shown in the following

$$\dot{W}_{net} = \dot{W}_T - \dot{W}_{pump} \tag{37}$$

Connections

Equation (38) shows the mass balance for Joint "A" shown in Figure 2

$$\dot{m}_{HTF,SF} = \dot{m}_{HTF,PB} + \dot{m}_{HTF,TES} \tag{38}$$

Furthermore, for Joint A we have

$$T_{out,SF} = T_{HTF,1} \tag{39}$$

$$T_{out,SF} = T_{HTF,3} \tag{40}$$

Equation (41) shows the energy balance for Joint "B" shown in Figure 2

$$\dot{m}_{HTF,TES} \cdot h_{HTF,2} + \dot{m}_{HTF,PB} \cdot h_{HTF,4} = \dot{m}_{HTF,SF} \cdot h_{in,SF} \tag{41}$$

It is worth mentioning that the set of equations is closed by including the thermodynamic property relations for HTF, solar salt and water.[28–30]

For the second case study, the amount of solar salt within the hot tank at the end of each time interval is considered to be the independent decision variable; consequently $[M_1{}^H, M_2{}^H, \ldots, M_{24}{}^H]$ constitute the set of decision variables.

Technical data concerning the second case study are gathered in Table 3. As shown in Figure 3, for the second case study, three solar radiation patterns with low, average, and high levels of DNI (the values are averaged over January, April, and June, respectively) are investigated.

Also, in this case a sinusoidal electricity price scenario (as defined by equation (42)) is considered.[31]

$$Price_t = 27 + 15\,sin\left(\frac{2\pi t - 15.4\pi}{24}\right) \tag{42}$$

Table 3. Technical data for the second case study.[9,10]

M_{min} (ton)	M_{max} (ton)	M_0^H (ton)	M_0^C (ton)	T_0^H (K)	T_0^C (K)	$(U \cdot A)_{exch,TES}$ (MW/K)	$\dot{m}_{fw,des}$ (kg/s)	k_p (Pa.s^2/kg^2)	$\eta_{T,des}$ (%)
2150	27920	15,000	15000	386	292	35	63.4	111.8	87.5
$P_{2,des}$ (bar)	$P_{3,des}$ (bar)	$\eta_{pump,des}$(%)	T_2 (K)	$T_{ss,1}$ (K)	$T_{out,SF}$ (K)	$(U \cdot A)_{exch,boiler}$ (MW/K)	em_o	$\dot{m}_{HTF,TES,des}$ (kg/s)	
90	0.08	75	370	386	390	5.06	−0.4	611.1	–

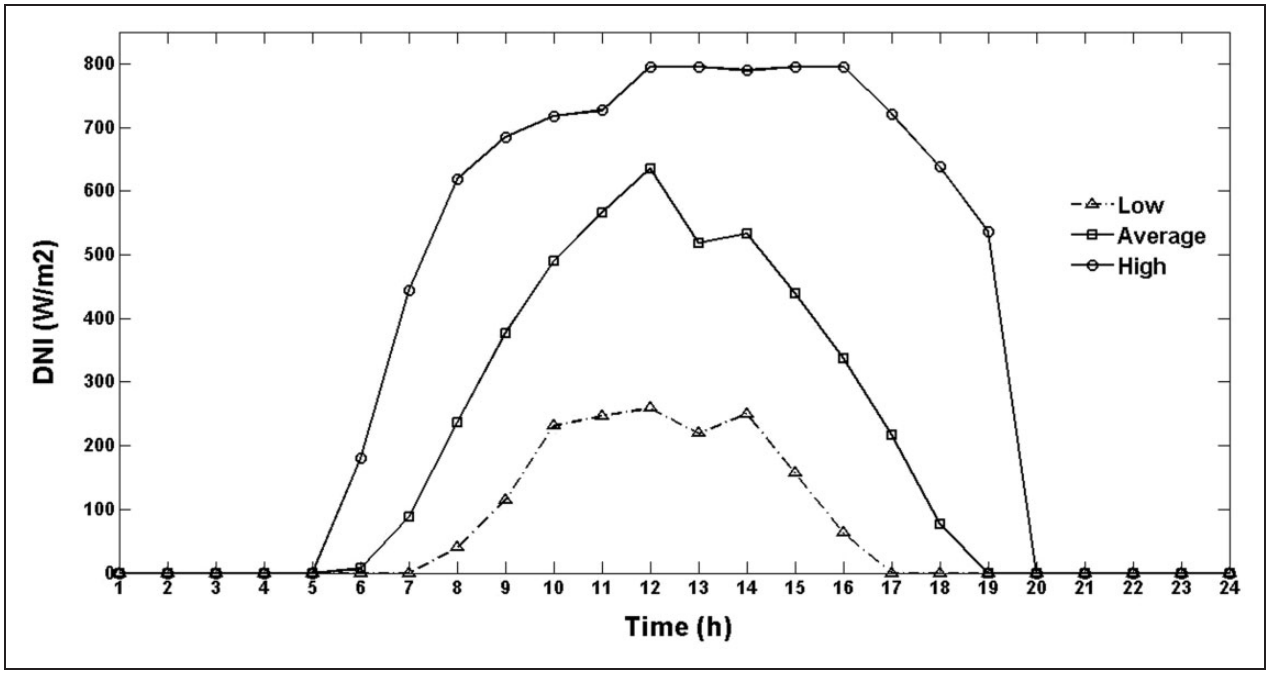

Figure 3. Solar radiation patterns (provided from Satel-light[32]).

Optimization algorithm (DP method)

The DP method has been described in some references.[25–27] This section explains how DP is applied to the problem under study. There is no difference in the DP procedure between the first and second case studies except that they have different sets of decision variables (i.e. $[Q_1{}^T, Q_2{}^T, \ldots, Q_{24}{}^T]$ for the first case study, and $[M_1{}^H, M_2{}^H, \ldots, M_{24}{}^H]$ for the second case study). Therefore, the DP approach is only explained for the first case study.

Before starting the DP procedure, the continuous range of each decision variable (i.e. the domain with the lower and upper bounds of Q^{Tmin} and Q^{Tmax}) must be discretized into a set of discrete values $\{Q^{Tmin},\ Q^{Tmin}+\Delta Q,\ Q^{Tmin}+2\Delta Q,\ \ldots, Q^{Tmax}\}$, where ΔQ denotes the step size of discretization. Accordingly, the optimal value of each decision variable is to be selected from the set of discrete values instead of the continuous range. If ΔQ is sufficiently small, the solution will be sufficiently close to the global optimum.

The DP procedure is schematically and mathematically shown in Figure 4 and equation (43), respectively.

It is worth noting that the initial amount of energy within the TES (Q_0^T) is considered to be a known value.

The revenue in a time interval,f_t, can be considered to be a function of only the amounts of energy within the TES at the beginning and at the end of that time interval (i.e. Q_{t-1}^T and Q_t^T, respectively). In other words, the other variables (Q_t^{TP}, Q_t^{ST} and Q_t^{SP}) are considered to be dependent variables based on equations (3) to (5).

$$\begin{aligned}
&\textit{First step}: \quad f_{0-2}(Q_2^T) = \max_{Q_1^T}\{f_1(Q_0^T, Q_1^T) + f_2(Q_1^T, Q_2^T)\}\\
&\textit{second step}: \quad f_{0-3}(Q_3^T) = \max_{Q_2^T}\{f_{0-2}(Q_2^T) + f_3(Q_2^T, Q_3^T)\}\\
&\qquad\qquad \vdots\\
&\textit{Last step}: \quad f_{0-24}(Q_{24}^T) = \max_{Q_{23}^T}\{f_{0-23}(Q_{23}^T) + f_{24}(Q_{23}^T, Q_{24}^T)\}
\end{aligned} \tag{43}$$

As shown in Figure 4, in the first step of the DP procedure, only the first two time intervals are considered. The total revenue from the beginning to the end of time interval 2 is the sum of the revenues in

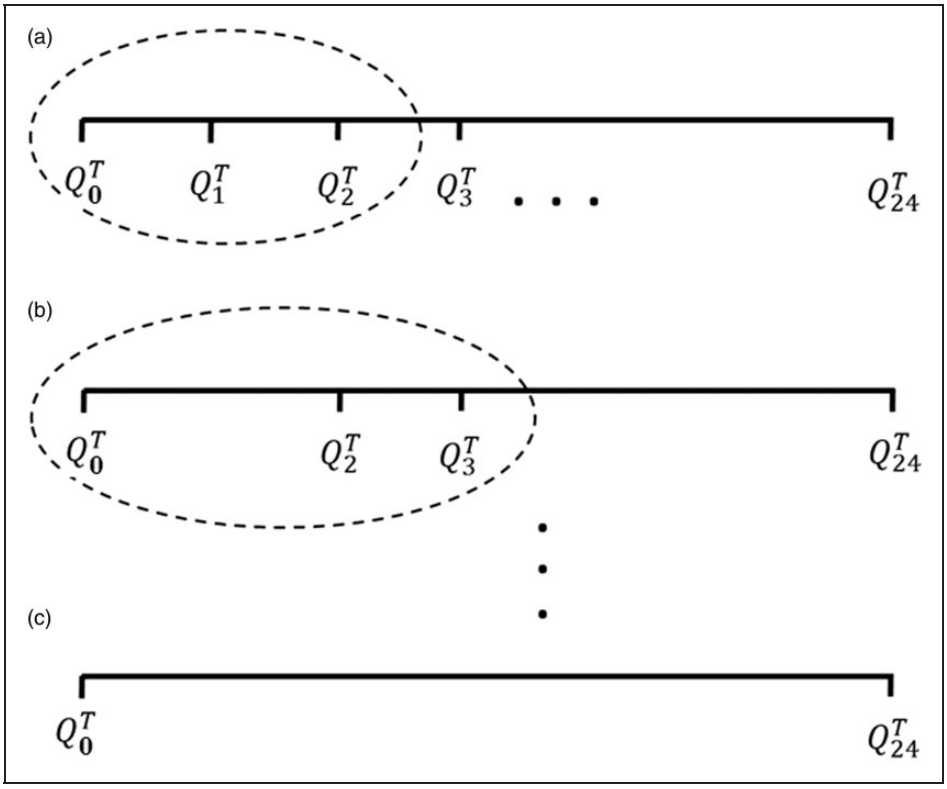

Figure 4. DP procedure. (a) first step (b) second step (c) last step.

time interval 1 ($f_1(Q_0^T, Q_1^T)$) and time interval 2 ($f_2(Q_1^T, Q_2^T)$). In this step, as shown in equation (43), for each discrete value of Q_2^T, the maximum possible revenue from the beginning to the end of time interval 2 (denoted by $f_{0-2}(Q_2^T)$) is found through examining all discrete values of Q_1^T. After this step, Q_1^T is no longer an independent decision variable because for each value of Q_2^T the best value of Q_1^T has been determined. Therefore, Q_1^T can be removed from the decision vector (as shown in Figure 4(b)). Since there are N discrete values of Q_2^T, and for each value of Q_2^T, N discrete values of Q_1^T must be examined, the order of computational complexity of this step is N^2.

In the second step, as shown in Figure 4(b), one more time interval is considered. In this step, as shown in equation (43), for each discrete value of Q_3^T, the maximum possible revenue from the beginning to the end of time interval 3 (denoted by $f_{0-3}(Q_3^T)$) is determined through examining all discrete values of Q_2^T. It is worth mentioning that $f_{0-2}(Q_2^T)$ has been computed in the previous step and does not need to be computed again. Moreover, Q_2^T is no longer an independent decision variable and can be removed from the decision vector. Similar to the first step, the order of computational complexity of this step is N^2.

The procedure continues until the maximum revenue from the beginning to the end of time interval 24 (denoted by f_{0-24}) is obtained as a function of only Q_{24}^T; hence, the maximum daily revenue can be obtained through examining all values of Q_{24}^T.

Since for each value of Q_t^T, the optimal value of Q_{t-1}^T has been determined during the DP steps, after the optimal value of Q_{24}^T is found, the optimal values of Q_{23}^T to Q_1^Tcan be obtained one by one through a back-tracking process.

Based on the previously described procedure, the DP method reduces the order of computational complexity from N^{24} (because there are 24 decision variables and each decision variable can take N discrete values) to $24N^2$.

Discussion and results

Results of the first case study (verification)

The developed program was executed by an Intel core i5 2.67 GHz processor.

Table 4 compares the results of the DP method obtained in the present study to those of the MILP method reported by Dominguez et al.[2] and indicates that the DP method achieved higher revenues. For example, the revenue obtained in the present work for the step size of $\Delta Q = 1$ MWh is approximately 1.3% higher than that reported by Dominguez et al.[2] As shown in Table 4, DP achieves greater revenues for finer ΔQ values at the expense of higher computation times.

Figure 5 illustrates the optimal set of decision variables (i.e. the optimal time variation of the amount of energy within the TES) and Figure 6 shows the corresponding time variation of the generated electrical

Table 4. Comparison between the present study and that of Dominguez et al.[2]

Step size ΔQ (MWh)	Computation time (s)	Optimum revenue in the present study ($) /$10^4$	Optimum revenue reported by Dominguez et al.[2] ($) /$10^4$	Improvement achieved in the present work (%)
1	139.0	3.873	3.825	+1.3
2	34.0	3.858	3.825	+0.9
4	8.5	3.857	3.825	+0.8
8	2.3	3.840	3.825	+0.4

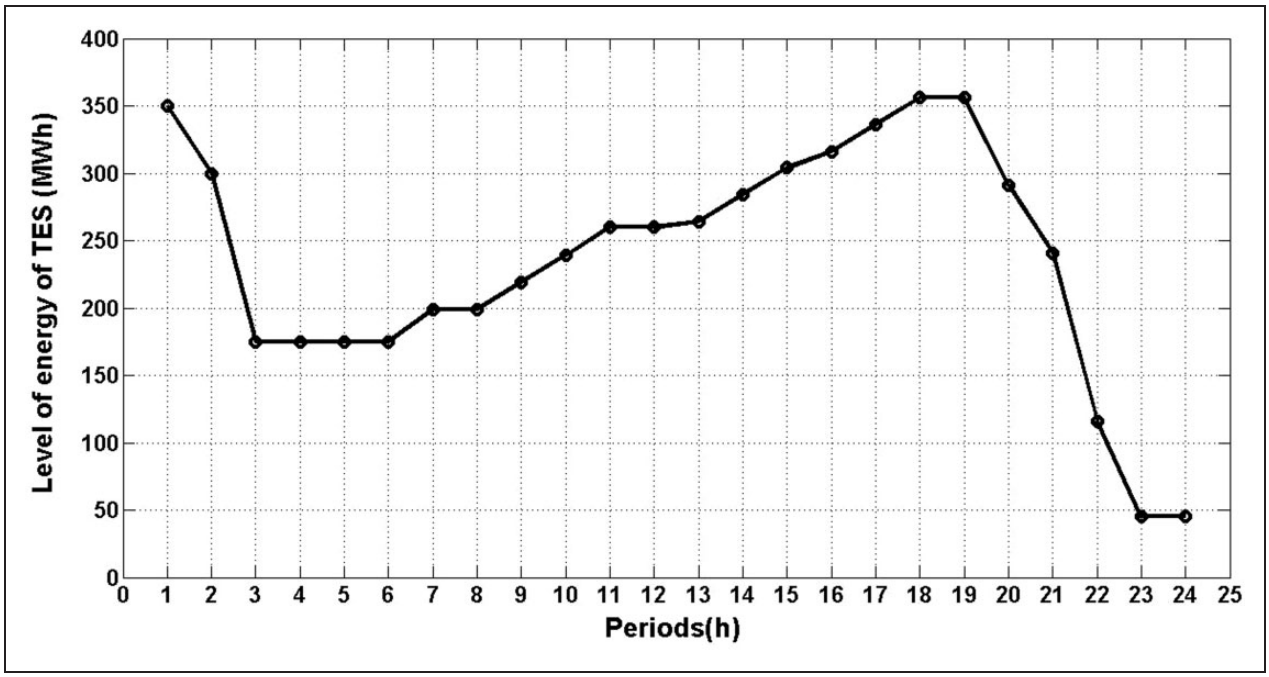

Figure 5. Optimal time variation of the amount of energy within the TES: the first case study.

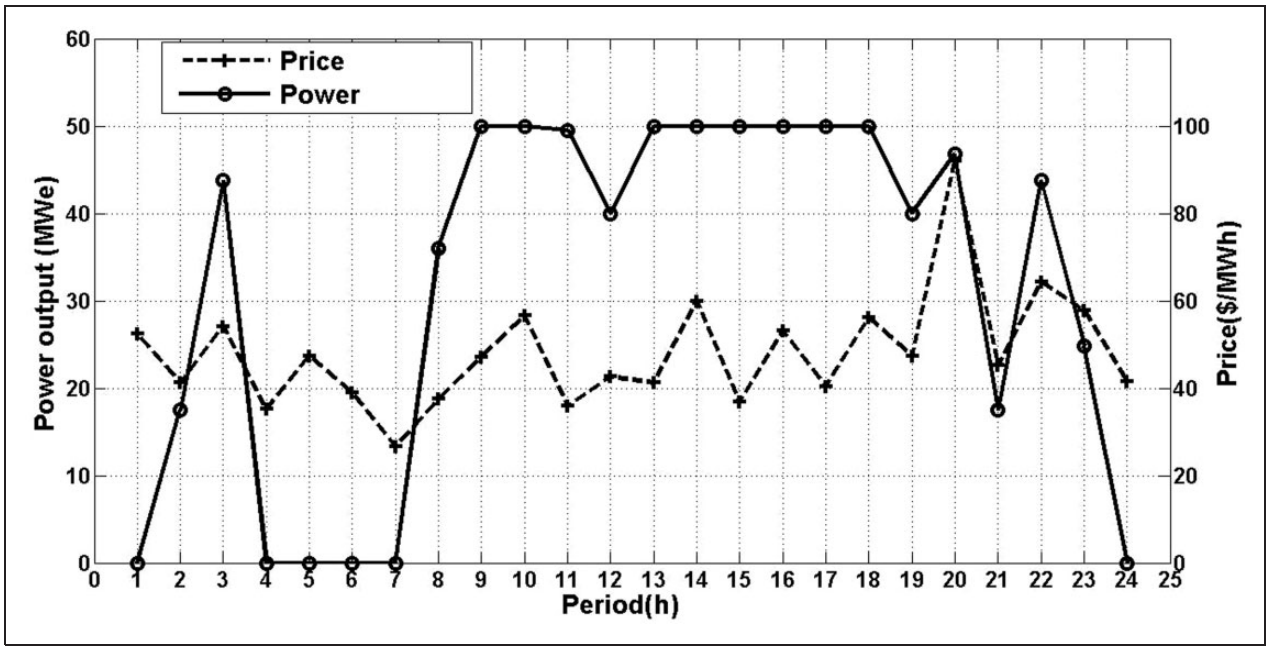

Figure 6. Price scenario and the optimal time variation of electrical power: the first case study.

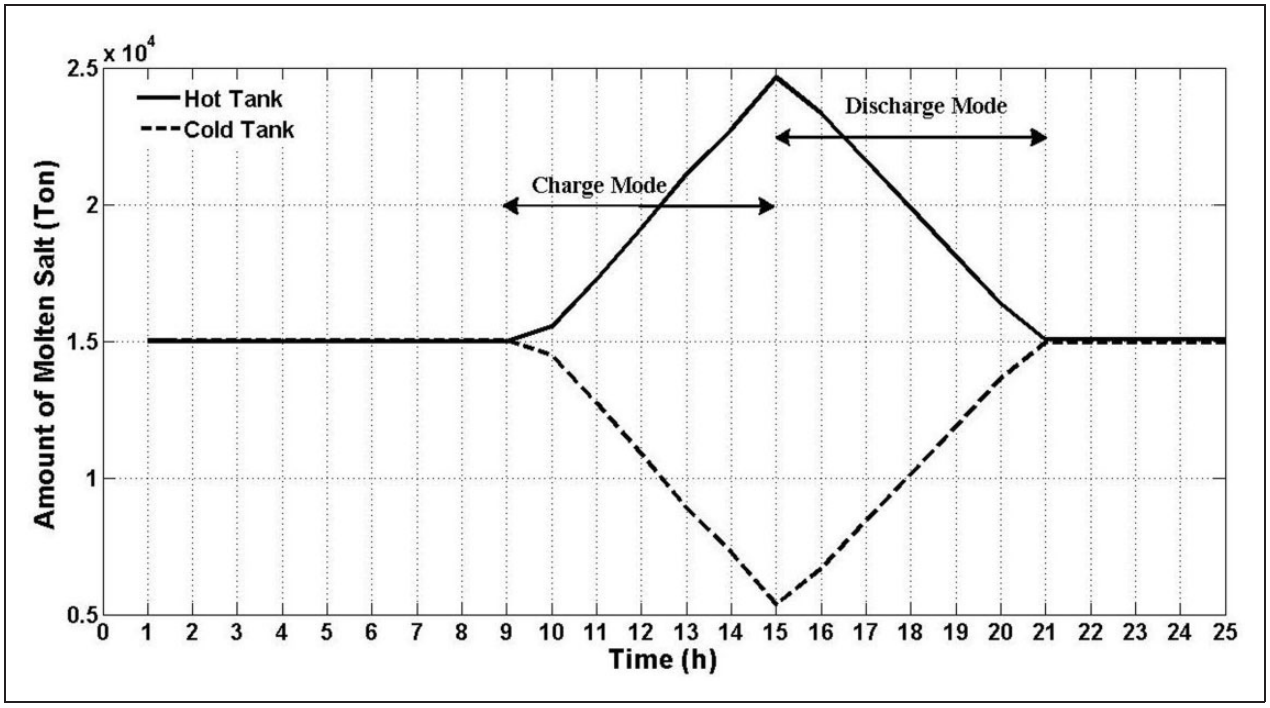

Figure 7. Optimal time variation of the amount of solar salt within the tanks: low DNI pattern.

power together with the price scenario. As shown in Figure 5, the level of energy within the TES reached the minimum allowable value ($Q^{T,min} = 45$ MWh) at the end of the operational period so as to generate as much electricity as possible. However, in the next case study, an added constraint is considered to avoid the depletion of the storage system at the end of the daily operational period. This constraint has not been considered for the first case study to have a fair comparison with Dominguez et al.[2]

Results of the second case study

For the second case study, the amount of solar salt within the hot tank at the end of the operational period is constrained to be greater than or equal to its initial value ($M_{24}^{H} \geqslant M_{0}^{H}$) to prevent the depletion of the TES system at the end of the operational period.

The second case study used the three levels of DNI shown in Figure 3. Results were obtained for the discretization step size of $\Delta M = 50$ton.

The results concerning the low DNI pattern are illustrated in Figures 7 and 8.

Figure 7 shows the optimal time variations of the amounts of solar salt within the hot and cold tanks with continuous and dashed lines, respectively. Since the total mass of solar salt is constant and the solar salt is only exchanged between the cold and hot tanks, the continuous and dashed lines in Figure 7 show a mirror like behavior. The ascending and descending parts of the continuous line in Figure 7 correspond to the charge and discharge operating modes, respectively.

As shown in Figure 7, the amount of solar salt within the hot tank approaches the minimum permissible value (i.e. the initial value) at the end of the operational period so as to generate as much electricity as possible.

Figure 8 illustrates the optimal time variation of power generation for the low DNI pattern. This figure shows that for achieving maximum revenue, the plant should work near full load condition (the power generation capacity is considered to be 60 MW) when it is active. This occurs because of the fact that the plant loses efficiency at partial load or off-design conditions. Equations (22), (27), (29), (31), and (36) govern the efficiency loss at part load conditions. Moreover, as observed in Figure 8, to achieve the highest revenue, the plant should be active around the times of high electricity prices.

Figures 9 and 10 show the results obtained for the average DNI pattern. These results resemble the results of the low DNI pattern except that the plant is active for a longer period of time.

Figures 11 and 12 relate to the high DNI pattern. In this case, as shown in Figure 11, the optimization procedure resulted in a more complex charge and discharge scenario. The corresponding time variation of power generation, shown in Figure 12, indicates that, as a result of the high DNI pattern, the plant is active most of the time except a few time intervals of low electricity prices.

The influence of the TES system on the daily revenue is investigated through eliminating the TES system from the second case study and comparing the results to those which have been previously obtained for the second case equipped with the TES system.

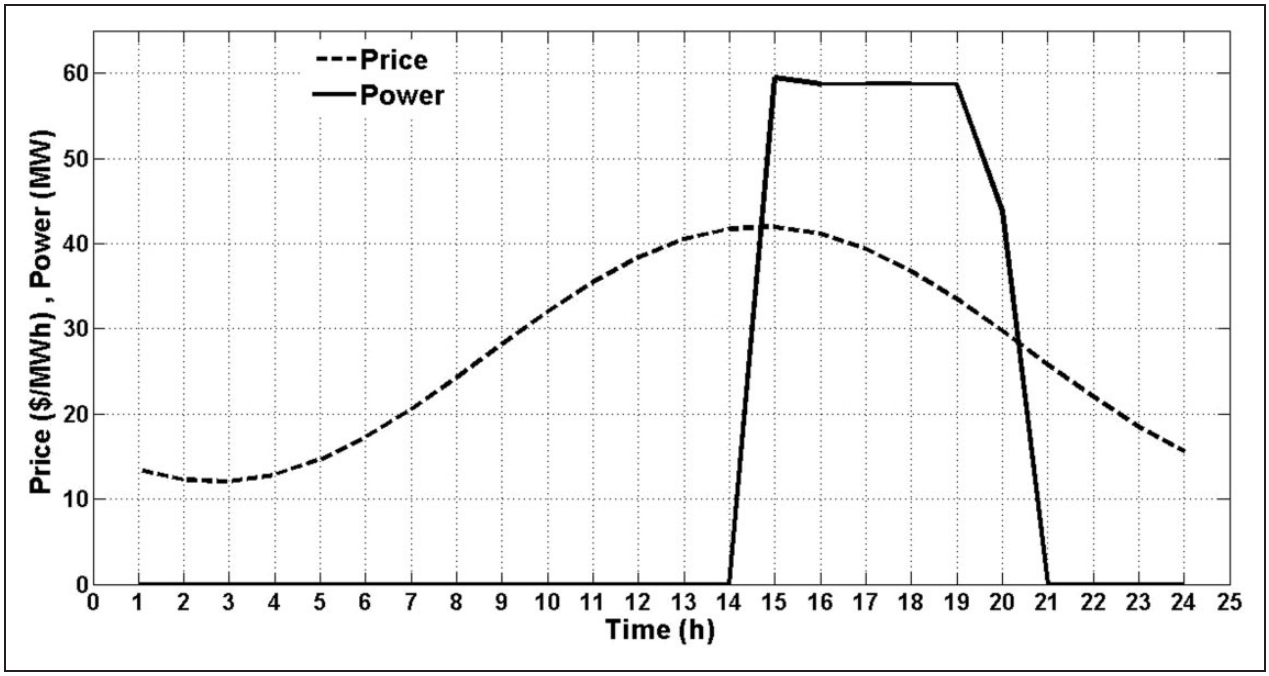

Figure 8. Electricity price scenario and the optimal time variation of power output: low DNI pattern.

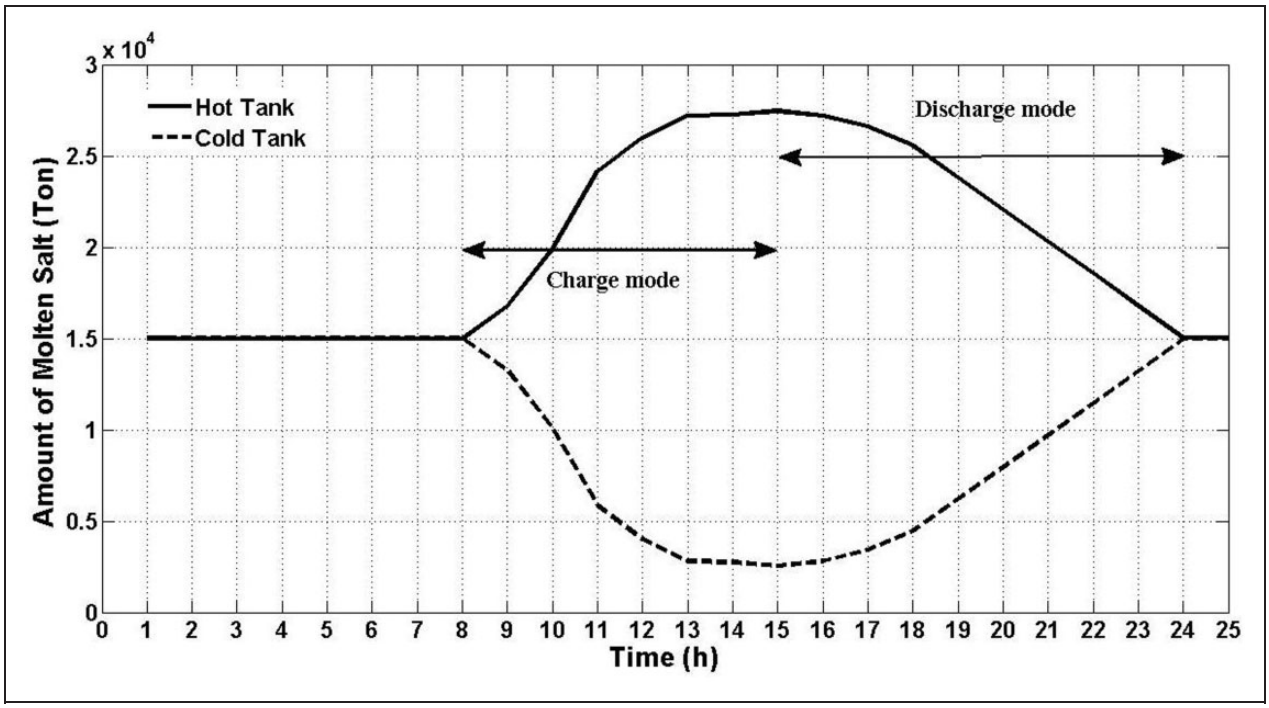

Figure 9. Optimal time variation of the amount of solar salt within the tanks: average DNI pattern.

As an illustration, Figure 13 compares power generation curves obtained for the cases with and without the TES system for the average DNI pattern. It is worth noting that for the plant without the TES system, the optimization procedure is not needed; instead, the hot HTF produced by the SF section is completely sent toward the PB to generate electricity; consequently, electricity can only be generated at the times with sufficient DNI values.

The influence of the TES system is quantitatively presented in Table 5. As shown in the table, the plant with the TES system, achieved the higher values of revenue. The difference percentage points are about 180%, 63%, and 37%, for the low, average, and high DNI patterns, respectively. The higher difference percentage points for the lower DNI levels occurs because under low DNI conditions, the plant without the TES system has to work under partial load

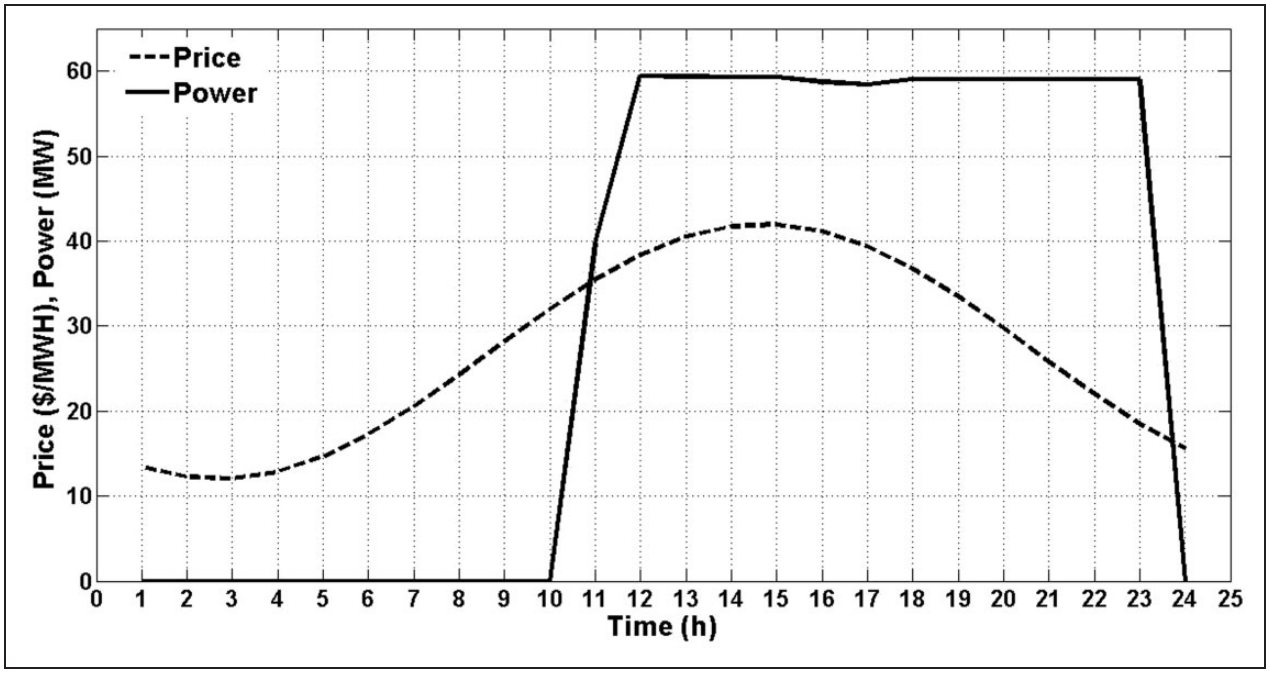

Figure 10. Electricity price scenario and optimal time variation of power output: average DNI pattern.

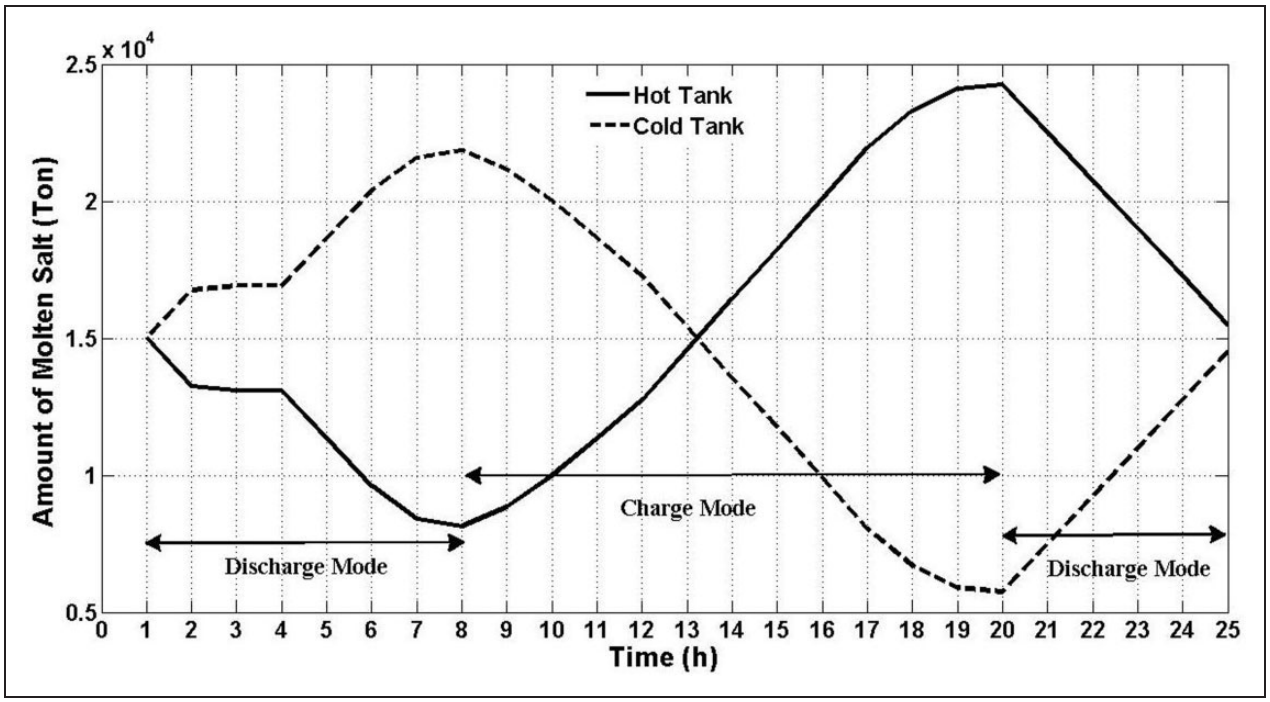

Figure 11. Optimal time variation of the amount of solar salt within the tanks: high DNI pattern.

conditions (i.e. far from the design conditions), thereby experiencing a substantial performance deficiency. But the plant with the TES system can accumulate the solar energy so that a sufficient amount of energy is available to drive the PB under its design conditions. As an illustration, this behavior is observed in Figure 7, where the plant is firstly charged during periods 9–11 and is then discharged to allow the plant to work near design conditions.

Conclusions

Dynamic programming guarantees the optimal solution and, therefore, is of great importance. This paper explained how DP is employed to optimize the performance of a CSP equipped with a TES system.

A benchmark case study with a simple thermal model was considered for verifying the developed optimization program. The present results showed a

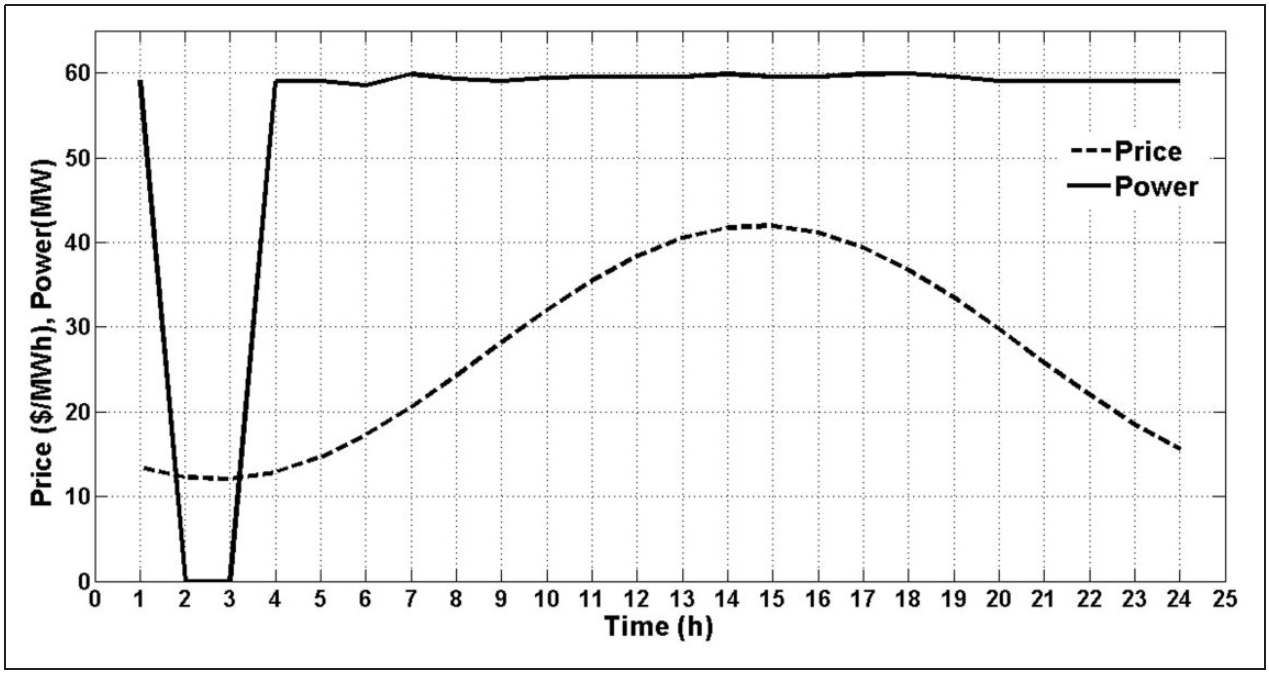

Figure 12. Electricity price scenario and optimal time variation of power output: high DNI pattern.

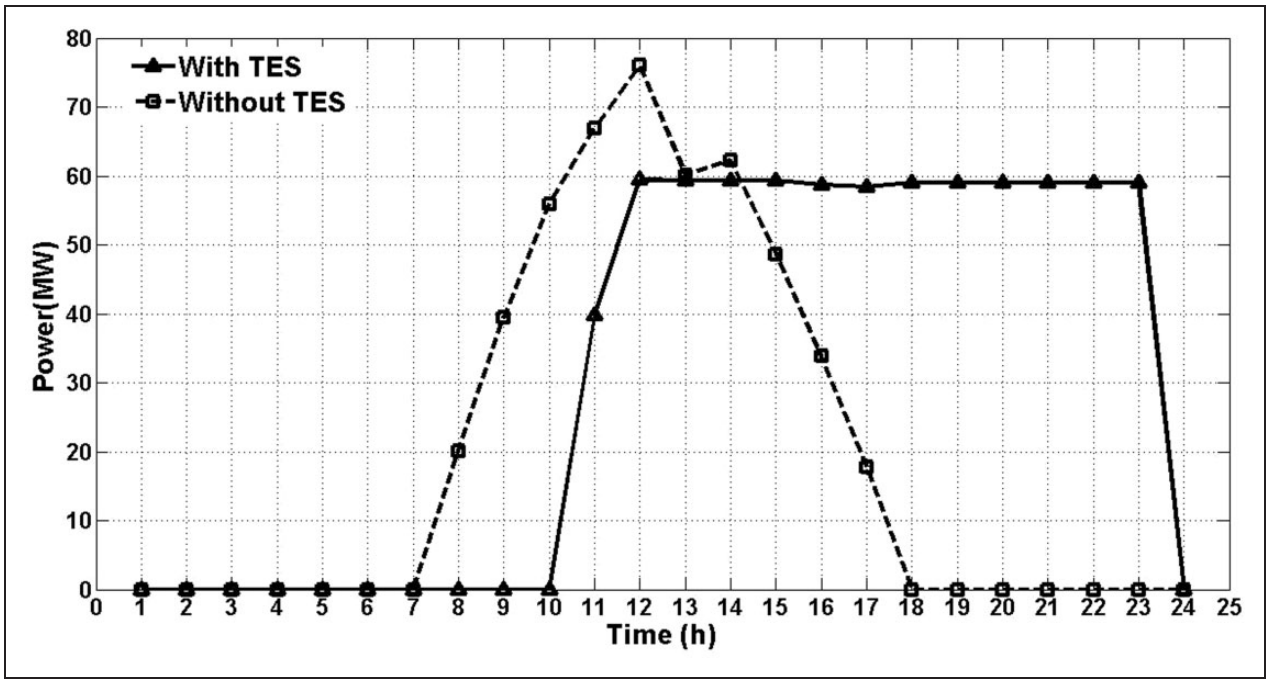

Figure 13. Comparison of power generation between the cases with and without the TES system.

Table 5. The influence of the TES system on daily revenue.

DNI level	Optimization run time (h)	Revenue for the case with TES system ($/day)	Revenue for the case without TES system ($/day)	The influence of TES system on revenue (%)
Low	1.7	12,650	4536	180
Average	3.4	25,600	15,709	63
High	5.5	37,077	27,009	37

slight improvement in the daily revenue in comparison with the literature.

To better simulate the real operation of a CSP, another case with a more detailed thermal model was also investigated. For all the three levels of daily solar radiation patterns studied, it was observed that to achieve maximum revenue, the CSP should work under base load conditions to avoid the performance deficiency occurring at partial load conditions; moreover, the CSP should work around the times of high electricity prices. However, the number of time intervals during which the CSP was active depended on the level of the solar radiation pattern.

Finally, a quantitative investigation revealed the considerable influence of the TES system on the daily revenue, especially for the lower levels of solar radiation pattern.

Declaration of Conflicting Interests

The author(s) declared no potential conflicts of interest with respect to the research, authorship, and/or publication of this article.

Funding

The author(s) received no financial support for the research, authorship, and/or publication of this article.

References

1. Barlev D, Vidu R and Stroeve P. Innovation in concentrated solar power. *Sol Energy Mat Sol C* 2011; 95: 2703–2725.
2. Dominguez R, Baringo L and Conejo AJ. Optimal offering strategy for a concentrating solar power plant. *Appl Energy* 2012; 98: 316–325.
3. Larraín T and Escobar R. Net energy analysis for concentrated solar power plants in northern Chile. *Renew Energy* 2012; 41: 123–133.
4. Atmaja TD and Pikra G. Absorber layer addition and thermal storage media comparison for concentrated solar power plant optimization. *Energy Procedia* 2013; 32: 74–83.
5. Lorente García I, Álvarez JL and Blanco D. Performance model for parabolic trough solar thermal power plants with thermal storage: Comparison to operating plant data. *Sol Energy* 2011; 85: 2443–2460.
6. IEA. *World energy outlook*. Paris: IEA Press, 2007.
7. IEA. *Competition in electricity markets*. Paris: IEA Press, 2007.
8. Jacobson MZ. Review of solutions to global warming, air pollution, and energy security. *Energy Environ Sci* 2009; 2: 148–173.
9. Rovira A, Montes MJ, Valdes M, et al. Energy management in solar thermal power plants with double thermal storage system and subdivided solar field. *Appl Energy* 2011; 88: 4055–4066.
10. Montes MJ, Abánades A, Martínez-Val JM, et al. Solar multiple optimization for a solar-only thermal power plant, using oil as heat transfer fluid in the parabolic trough collectors. *Sol Energy* 2009; 83: 2165–2176.
11. Lizarraga-Garcia E, Ghobeity A, Totten M, et al. Optimal operation of a solar-thermal power plant with energy storage and electricity buy-back from grid. *Energy* 2013; 51: 61–70.
12. Martín L and Martín M. Optimal year-round operation of a concentrated solar energy plant in the south of Europe. *Appl Therm Eng* 2013; 59: 627–633.
13. Kost C, Flath CM and Möst D. Concentrating solar power plant investment and operation decisions under different price and support mechanisms. *Energ Policy* 2013; 61: 238–248.
14. Baghernejad A and Yaghoubi M. Exergoeconomic analysis and optimization of an Integrated Solar Combined Cycle System (ISCCS) using genetic algorithm. *Energy Convers Manage* 2011; 52: 2193–2203.
15. Cabello JM, Cejudo JM, Luque M, et al. Optimization of the size of a solar thermal electricity plant by means of genetic algorithms. *Renew Energy* 2011; 36: 3146–3153.
16. Soltani R, Mohammadzadeh Keleshtery P, Vahdati M, et al. Multi-objective optimization of a solar-hybrid cogeneration cycle: Application to CGAM problem. *Energy Convers Manage* 2014; 81: 60–71.
17. Silva R, Berenguel M, Pérez M, et al. Thermo-economic design optimization of parabolic trough solar plants for industrial process heat applications with memetic algorithms. *Appl Energy* 2014; 113: 603–614.
18. Marano V, Rizzo G and Tiano FA. Application of dynamic programming to the optimal management of a hybrid power plant with wind turbines, photovoltaic panels and compressed air energy storage. *Appl Energy* 2012; 97: 849–859.
19. Pop PC. *Generalized network design problems: Modeling and optimization*. Berlin: De Gruyter, 2012.
20. Slawomir Koziel XSY. *Computational optimization, methods, and algorithms*. Heidelberg: Springer, 2011.
21. Venter G. Review of optimization techniques. *Encyclopedia of aerospace engineering*. New York: John Wiley and Sons, Ltd, 2010.
22. Nocedal J and Wright SJ. *Numerical optimization*. New York: Springer, 1999.
23. Talbi EG. *Metaheuristics: From design to implementation*. Chichester: John Wiley & Sons, 2009.
24. Yang XS. *Nature-inspired metaheuristic algorithms*. Frome, UK: Luniver Press, 2010.
25. Bellman R. *Dynamic programming*. Princeton: NJ University Press, 1957.
26. Carter RG. Pipeline optimization: Dynamic programming after 30 years. In: *30th annual meeting pipeline simulation interest group (PSIG)*, Houston, TX, USA, 1998.
27. Sanaye S and Mahmoudimehr J. Minimization of fuel consumption in cyclic and non-cyclic natural gas transmission networks: Assessment of genetic algorithm optimization method as an alternative to non-sequential dynamic programing. *J Taiwan Inst Chem Eng* 2012; 43: 904–917.
28. Ferri R, Cammi A and Mazzei D. Molten salt mixture properties in RELAP5 code for thermodynamic solar applications. *Int J Therm Sci* 2008; 47: 1676–1687.
29. IAPWS. Release on the IAPWS industrial formulation for the thermodynamic properties of water and steam. The International Association for the Properties of Water and Steam (IAPWS), 1997.

30. Solutia, http://www.therminol.com/pages/products/vp-1.asp (2014, accessed 15 March 2014).
31. Zhao G and Davison M. Optimal control of hydroelectric facility incorporating pump storage. *Renew Energy* 2009; 34: 1064–1077.
32. Satel-light, http://www.satel-light.com (2014, accessed 8 March 2014).

Appendix

Notation

DNI	direct normal irradiance (W/m^2)
h	specific enthalpy (kJ/kg)
M	amount of solar salt in storage tank (ton)
$\dot{m}$	mass flow rate (kg/s)
P	pressure (kPa)
P^{max}	power generation capacity (MW-e)
$Price$	electricity price ($/MWh)
P^{Total}	generated electrical power (MW-e)
$\dot{Q}^{P,max}$	maximum permissible amount of thermal power received by PB (MW)
$\dot{Q}^{P,min}$	minimum permissible amount of thermal power received by PB (MW)
$\dot{Q}^{SP}$	thermal power sent from SF to PB (MW)
$\dot{Q}^{S}$	thermal power generated in SF (MW)
$\dot{Q}^{ST}$	thermal power sent from SF to TES (MW)
Q_t^T	amount of energy within TES at the end of time interval t (MWh)
$Q^{T,max}$	maximum permissible amount of energy in TES (MWh)
$Q^{T,min}$	minimum permissible amount of energy in TES (MWh)
$\dot{Q}^{TP}$	thermal power sent from TES to PB (MW)
R^{Ch}	ramp-up limit (MW-e/h)
R^{Dis}	ramp-down limit (MW-e/h)
SS	solar salt
u	specific internal energy (kJ/kg)
U	binary value indicating the on/off state of PB (–)
$\dot{W}$	power (MW)
ΔQ	step size of discretization (MWh)
Δt	time step (h)
ΔT_{LM}	logarithmic mean temperature difference (°C)
η_1	conversion efficiency of thermal energy of SF to electricity (–)
η_2	conversion efficiency of thermal energy of TES to electricity (–)
η_3	conversion efficiency of thermal energy of SF to thermal energy of TES (–)
η_{pump}	pump efficiency (–)
η_T	turbine efficiency (–)
υ_f	liquid water specific volume (m^3/kg)

Subscript

HTF	heat transfer fluid